THE JOURNAL OF PHYSICAL CHEMISTRY C

Article

pubs.acs.org/JPCC

Equilibrium Adsorption of D- and L-Alanine Mixtures on Naturally Chiral Cu{3,1,17}$^{R\&S}$ Surfaces

Yongju Yun,[†] Daniel Wei,[‡] David S. Sholl,[‡] and Andrew J. Gellman*,[†]

[†]Department of Chemical Engineering, Carnegie Mellon University, Pittsburgh, Pennsylvania 15213, United States

[‡]School of Chemical and Biomolecular Engineering, Georgia Institute of Technology, Atlanta, Georgia 30332-0100, United States

Supporting Information

ABSTRACT: Equilibrium adsorption of gas phase mixtures of D- and L-alanine (Ala) onto the naturally chiral Cu{3,1,17}$^{R\&S}$ surfaces has been studied by both experiment and DFT-based modeling. Isotopically labeled *L-Ala ($HO_2{}^{13}CCH(NH_2)CH_3$) and unlabeled D-Ala allow mass spectrometric enantiodifferentiation of the adsorbed species during temperature-programmed decomposition, following equilibrium adsorption. Measurements of the relative equilibrium coverages of D- and *L-Ala on the Cu{3,1,17}$^{R\&S}$ surfaces, $\theta_{D/R}/\theta_{*L/R} = \theta_{*L/S}/\theta_{D/S}$, at gas phase partial pressure ratios of $P_{*L}/P_D = 1/2$, 1, and 2 indicate that the D-Ala and *L-Ala conglomerate phases are more energetically stable than a D*L-Ala racemate phase, but that their adsorption energies are not measurably enantiospecific, $\Delta\Delta E_{DL} \approx 0$. Although the DFT simulations provide a self-consistent structure of Ala overlayers on Cu{3,1,17}$^{R\&S}$ they overestimate the enantiospecificity of the adsorption energetics.

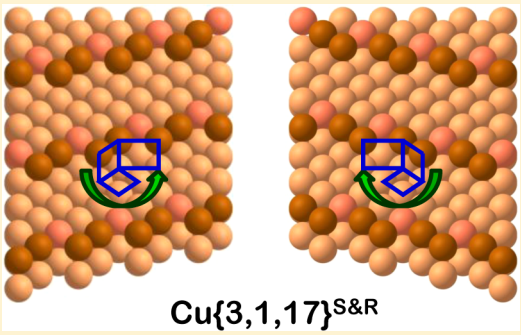

1. INTRODUCTION

A characteristic hallmark of life on Earth is the homochirality of biomolecules such as amino acids, sugars, proteins, and DNA.[1,2] One of its consequences is that in the homochiral environment of living organisms, the two enantiomers of a chiral molecule can exhibit significantly different physiological effects.[3−5] This creates an enormous >$200B/yr market for enantiomerically pure compounds such as pharmaceuticals.[6] As a result, enantioselective chemical processes have attracted a great deal of attention in the biochemical and pharmaceutical industries. As one route to enantioselectivity, chiral surfaces are attractive media for chiral separations and for enantioselective heterogeneous catalysis, if enantioselectivity can be achieved by catalytically active materials such as metals.

Single enantiomer chiral surfaces can be created by several means. The most common is the irreversible adsorption of enantiomerically pure, chiral organic molecules on achiral metal surfaces, thereby rendering the surfaces chiral.[7−10] Such surfaces can then serve as enantiospecific adsorbents or catalysts; however, their chemical and thermal stability is limited by the intrinsic stability of the organic modifier. Simple metal surfaces themselves can be much more stable and more catalytically active than organically modified surfaces, if they can be prepared in intrinsically chiral form. Although the bulk crystal structures of metals are achiral, intrinsically chiral surfaces can be obtained from metals by exposing their low symmetry, high Miller index planes.[11−13] Because the terrace-step-kink structures of these surfaces lack symmetry, they are not superimposable on their mirror images and, therefore, they are chiral. Enantiospecific properties of chiral molecules on naturally chiral metal surfaces have been widely studied by various methods.[14−19] When adsorbed on naturally chiral surfaces, chiral molecules exhibit enantiospecific desorption kinetics,[14,20−22] reaction kinetics,[23,24] orientations,[25,26] and electrochemistry.[27,28]

Recently, Yun et al. reported the first unequivocal observation of the enantioselective separation of a racemic mixture on a naturally chiral metal surface.[29] That work made use of ^{13}C-labeling in the *L-aspartic acid (*L-Asp, the asterisk (*) herein refers to the isotopically labeled species) to enable mass spectrometric enantiodiscrimination of D-Asp from *L-Asp during adsorption from the gas phase and subsequent decomposition/desorption of the adsorbed phase. The equilibrium adsorption of a gas phase, racemic mixture of D- and *L-Asp on naturally chiral Cu{3,1,17}$^{R\&S}$ surfaces resulted in ∼39% surface enantiomeric excess (ee_s) in the adsorbed phase, favoring adsorption of D-Asp over *L-Asp on the Cu{3,1,17}^{S} surface (and vice versa on the Cu{3,1,17}^{R} surface). The quantitative nature of this isotope labeling method allowed direct determination of the ratios of the enantiospecific adsorption equilibrium constants for D- and *L-Asp on the Cu{3,1,17}$^{R\&S}$ surfaces, $K_{*L/R}/K_{D/R} = K_{D/S}/K_{*L/S} = 2.29 \pm 0.17$, and estimation of the enantiospecific difference in the free energies of adsorption, $\Delta\Delta G_{DL} = 3.15 \pm 0.29$ kJ/mol. The ^{13}C-labeling methodology developed for the study of Asp/Cu{3,1,17}$^{R\&S}$ should be generally applicable to the study of enantiospecific adsorption of any enantiomers for which one of the two can be obtained in an isotopically labeled form, that is,

Received: April 17, 2014
Revised: June 11, 2014
Published: June 13, 2014

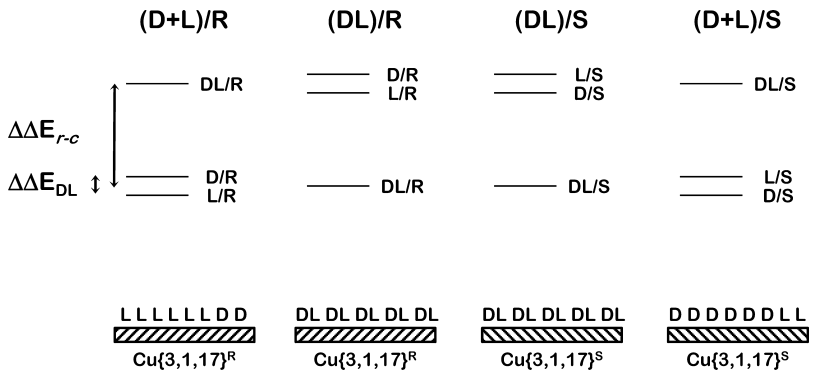

Figure 1. Illustration of the energetics and possible phases for D- and L-Ala coadsorption on Cu{3,1,17}$^{R\&S}$ surfaces from gas phase mixtures of the two enantiomers. The (D + L)/R scenario shows the case of exposure of the Cu{3,1,17}^{R} surface to a gas phase mixture of D- and L-Ala. In the adsorbed state, the enantiomerically pure, L-Ala conglomerate phase is more energetically stable than the D-Ala conglomerate by $\Delta\Delta E_{DL}$. The conglomerate phases are much more energetically stable than the DL-Ala racemate phase by $\Delta\Delta E_{r-c} \gg \Delta\Delta E_{DL}$. In the (DL)/R scenario, the DL-Ala racemate phase is much more stable than either of the enantiomerically pure conglomerate phases. The (D + L)/S and (DL)/S scenarios illustrate the analogous situations for adsorption on the Cu{3,1,17}^{S} surface. In the fourth panel with $\Delta\Delta E_{r-c} \gg \Delta\Delta E_{DL}$, the D-Ala is adsorbed preferentially.

most amino acids. The work described herein has applied the ^{13}C-labeling method to study the enantiospecific surface chemistry of alanine ($HO_2CCH(NH_2)CH_3$, Ala), the simplest chiral amino acid, on the Cu{3,1,17}$^{R\&S}$ surfaces.

Adsorption of Ala on Cu surfaces has been extensively studied as a model system for understanding the surface chemistry of chiral biomolecules such as amino acids on metal surfaces. Previous studies using reflection absorption infrared spectroscopy (RAIRS) have shown that Ala adsorbs on Cu surfaces in its anionic form ($-O_2CCH(NH_2)CH_3$).[30−40] Low energy electron diffraction (LEED), near edge X-ray absorption fine structure spectroscopy (NEXAFS), and scanning tunneling microscopy (STM) have been used to show that enantiomerically pure D- and L-Ala adsorbed on the naturally chiral Cu{531}^{R} surface exhibit enantiospecific differences in their adsorption geometries and long-range order.[18,26] Furthermore, Clegg et al. showed that adsorption of D- and L-Ala leads to enantiospecific reconstruction of a naturally chiral Cu{531}^{S} surface.[41] The greater goal of this type of work is to understand the origin of the enantiospecific differences in the energetics of chiral adsorbates on chiral surfaces. These are the root cause of enantioselectivity in processes such as separations and catalysis. However, the direct quantitative measurement of enantiospecific energy differences of chiral adsorbates on chiral surfaces is experimentally challenging. Despite extensive studies of Ala on chiral Cu surfaces, adsorption enantioselectivity has been predicted only on the basis of computational modeling.[42,43]

In this work, we describe direct measurements of the equilibrium adsorption of D- and *L-Ala mixtures on naturally chiral Cu{3,1,17}$^{R\&S}$ surfaces. In the event of enantiospecific adsorption, the enantiomer with the higher adsorption energy on a chiral surface equilibrates at a higher coverage than the other enantiomer. By controlling the ratio of enantiomers in the gas phase, P_D/P_{*L}, and measuring the ratio of the coverages in the adsorbed phase, θ_D/θ_{*L}, one can detect enantioselective separation and quantify the enantiospecific difference in the adsorption energies of two enantiomers on the chiral surface.[29] The challenge in measuring the relative coverages of two enantiomers adsorbed on the surface arises from the lack of a method for enantiodiscrimination of molecules once adsorbed. In this work, the D- and *L-Ala are distinguished using mass spectrometry and ^{13}C-labeling of the *L-Ala. This novel method allows us to investigate enantiospecific adsorption over a range of relative partial pressures of two enantiomers in the gas phase.

The model considered in this work for interpreting the equilibrium adsorption of D- and *L-Ala enantiomers is more complex than that needed to describe the adsorption of D- and *L-Asp on the Cu{3,1,17}$^{R\&S}$ surfaces.[29] In the case of D- and *L-Asp, the adsorbed monolayer was well described as consisting of domains of enantiomerically pure conglomerate phases, or equivalently a random solution of noninteracting enantiomers. No explicit consideration was given to the possible formation of an adsorbed racemate phase of D*L-Asp; nor was this necessary to interpret their behavior observed on Cu{3,1,17}$^{R\&S}$. Bulk crystallization of racemic mixtures of many chiral compounds, including both DL-Asp and DL-Ala, results in the formation of racemate phases, crystals in which each unit cell contains an equal number of both the D- and the L-enantiomer.[44,45] The formation of enantiomerically pure conglomerates, physical mixtures of crystals in which each individual crystal is enantiomerically pure, is relatively rare. Thus, the possible formation of 2D racemate domains during adsorption of a racemic mixture onto a surface should be considered. Our DFT calculations of the adsorption energies of conglomerate and racemate phases of D, L, and DL-Ala on Cu{3,1,17}$^{R\&S}$ suggest that they are of comparable energy and, therefore, that both phases should be considered. Figure 1 illustrates the framework for thinking about the work presented. The figure shows four scenarios for the relative energetics of the D-conglomerate, the L-conglomerate and the DL-racemate that might form as a result of the adsorption of a mixture of D- and L-Ala on the Cu{3,1,17}$^{R\&S}$ surfaces. In the first scenario, (D + L)/R, the L-conglomerate is energetically more stable than the D-conglomerate, and both are much more stable than the DL-racemate, $\Delta\Delta E_{r-c} \gg \Delta\Delta E_{DL}$. Here, $\Delta\Delta E_{DL}$ is the difference in the adsorption energies of the D- and L-Ala conglomerate phases on Cu{3,1,17}^{R} and $\Delta\Delta E_{r-c} = \Delta E_{rac} - {}^{1}/_{2}(\Delta E_D + \Delta E_L)$ is the difference in the adsorption energies of the racemate phase and conglomerate phases. As shown at the bottom of Figure 1, exposure of the Cu{3,1,17}^{R} surface to a racemic mixture of D- and L-Ala in the gas phase would result in predominantly conglomerate phase adsorption with an excess of the L-Ala phase. Note that the relative coverage of the enantiomers would depend on the ratio of their partial pressures in the gas phase, $\theta_{D/R}/\theta_{L/R} = K_{D/R}P_D/K_{L/R}P_L$.[29]

The situation is mirrored diastereometrically in the scenario (D + L)/S. In the (DL)/R and (DL)/S scenarios, the DL-racemate is energetically much more stable than either of the conglomerate phases. As shown at the bottom of Figure 1, during exposure of either Cu{3,1,17}$^{R\&S}$ surface to a mixture in the gas phase, the relative coverages of the adsorbed enantiomers is $\theta_{D/R}/\theta_{L/R} = 1$ and independent of the relative enantiomer partial pressures.

The work described in this paper develops and demonstrates a methodology for distinguishing between conglomerate and racemate adsorption. The relative equilibrium coverages of the D- and *L-Ala during exposure to gas phase mixtures with $P_D/P_{*L} = 1/2$, 1, and 2 reveal that the adsorbed phase forms enantiomerically pure D- and *L-Ala conglomerates that are energetically much more stable than the D*L-Ala racemate phase. Furthermore, both enantiopure phases have the same energetic stability on Cu{3,1,17}$^{R\&S}$ surfaces, $\Delta\Delta E_{DL} = 0$. Experimentally measured thermodynamic properties such as $K_{D/R}/K_{*L/R} = K_{*L/S}/K_{D/S}$ have been compared to values predicted by dispersion corrected DFT calculations. These experimental and computational studies provide insight into the enantioselectivity of chiral amino acid adsorption on naturally chiral surfaces.

2. EXPERIMENTAL SECTION

Study of enantioselective adsorption of D- and *L-Ala on Cu{3,1,17}$^{R\&S}$ surfaces was performed in an ultrahigh vacuum, surface analysis chamber with a base pressure of 2×10^{-10} Torr. The chamber is equipped with an Ar^+ ion sputter gun to clean the Cu{3,1,17}$^{R\&S}$ surfaces, LEED optics to examine the ordering of clean surfaces, a homemade evaporator to deposit Ala on the Cu single crystal surfaces, and an Extrel mass spectrometer to detect species in the gas phase and those desorbing from the surface.

The Cu{3,1,17} single crystal sample (Monocrystals Company) was approximately 10 mm in diameter and 2 mm thick. The Cu single crystal disk exposed the Cu{3,1,17}^{R} surface on one side and the Cu{3,1,17}^{S} surface on the other side. The temperature of the sample was controlled within the range 90−1000 K by resistive heating and liquid nitrogen cooling and was measured using a chromel−alumel thermocouple spot-welded to its edge. The temperature was controlled by a computer monitoring the temperature and varying the heating current. The Cu sample was cleaned by repeated cycles of 1 keV Ar^+ ion sputtering while annealing at 850 K for 500 s. In the final step of the sputtering-annealing procedure, the sample was cooled at a controlled rate of −1 K/sec at a pressure of $<1 \times 10^{-9}$ Torr in order to obtain a well-ordered surface structure. The long-range order of the clean Cu{3,1,17}$^{R\&S}$ surfaces was verified by LEED before adsorption of Ala.

Unlabeled D-Ala (Alfa Aesar, 99% chemical and optical purity) and isotopically labeled *L-Ala ($HO_2{}^{13}CCH(NH_2)CH_3$, Cambridge Isotope Laboratories, 98% chemical purity, 99 atom %) were vapor deposited onto the Cu{3,1,17}$^{R\&S}$ surfaces by sublimation from a homemade Knudsen cell evaporator with two glass vials; one for each enantiomer. The glass vials were wrapped with resistance heating wires and their temperatures were measured by thermocouples bonded to their exteriors. The fluxes of D- and *L-Ala from each vial were controlled independently by heating the vials to different temperatures. The time of exposure of the Cu{3,1,17}$^{R\&S}$ surfaces to the D- and *L-Ala vapors was controlled by opening and closing a shutter placed in front of the glass vials. After exposure to Ala, the sample was positioned in front of the aperture to the mass spectrometer and then heated at 1 K/s to conduct temperature-programmed reaction spectroscopy of the adsorbed species. The relative coverages of D- and *L-Ala on the Cu{3,1,17}$^{R\&S}$ surfaces were determined by monitoring the signals for CO_2 ($m/q = 44$) and $^{13}CO_2$ ($m/q = 45$) with the mass spectrometer while heating the surfaces from 250 to 670 K at 1 K/s.

3. COMPUTATIONAL METHODS

Computational simulations of D- and L-Ala on Cu{3,1,17}^{S} were carried out using periodic DFT calculations using the Vienna ab initio simulation package (VASP).[46−49] The PBE-GGA functional was used to describe the electron−electron exchange and correlation interactions while core−electron interactions were described with the projector augmented-wave (PAW) potential.[50−53] A plane wave expansion cutoff of 500 eV was used for all calculations. Structural optimization, performed by a conjugate gradient algorithm, was considered converged with a force stopping criterion of 0.03 eV/Å. The effects of long range dispersion forces were accounted for through Grimme's D2 dispersion correction method.[54] The interatomic spacing of Cu was obtained through modeling of bulk fcc Cu atoms with a supercell containing 8 Cu atoms in an FCC lattice using 16 × 16 × 16 k-points. The construction of a Cu{3,1,17}^{S} slab was similar to earlier work by Rankin and Sholl.[55] The surface consisted of a single Cu{3,1,17}^{S} surface unit cell with a vacuum spacing of at least 10 Å. The surface slab was 7 Å thick with the bottommost 3 Å constrained in bulk positions. All calculations were performed with a Monkhorst−Pack grid of 4 × 4 × 1 k-points. The Ala was adsorbed in the deprotonated form with a tridentate footprint.[33−40] A dense adlayer was defined as two Ala molecules coadsorbed on the surface unit cell. To ensure a systematic examination of the surface, we modified the *n_A_x* denotation of the adlayer defined by Rankin and Sholl to be *m_n_A_x*.[55] Here, the *m* denotes whether the adlayer was enantiopure (D- or L-) or racemic (DL-) Ala.

4. RESULTS

4.1. LEED Patterns of the Clean Cu{3,1,17}$^{R\&S}$ Surfaces.

The chirality of the Cu{3,1,17}$^{R\&S}$ surface structures was verified using LEED. Figure 2 shows the ideal structures of the Cu{3,1,17}$^{R\&S}$ surfaces in the top panels and the LEED patterns obtained from the clean Cu{3,1,17}$^{R\&S}$ surfaces in the lower panels. The ideal atomic structures of the Cu{3,1,17}$^{R\&S}$ surfaces have monatomic kinked steps formed by (110) and (111) microfacets, and separated by (100) terraces. Although it is known that the real structures of such high Miller index surfaces are subject to thermal roughening,[56−58] STM imaging of Cu{643}^{R} and Cu{531}^{S} surfaces have shown that the net chirality of the surfaces is preserved.[13,59] Although thermal roughening of the steps results in the coalescence of kinks and loss of the periodic distribution of kinks along the step edge, the chirality of the remaining kinks is the same as that of the ideal surface structure. LEED patterns from high Miller index surfaces with kinked steps have periodicity based on that of the terraces but modified by splitting of the diffraction spots due to the presence of the step edges.[60] The LEED patterns of the clean Cu{3,1,17}$^{R\&S}$ surfaces (Figure 2) display the square symmetry of the (100) terraces with obvious spot splitting. The split spots in the diffraction patterns are misoriented from the low Miller index directions, indicating that the steps run along

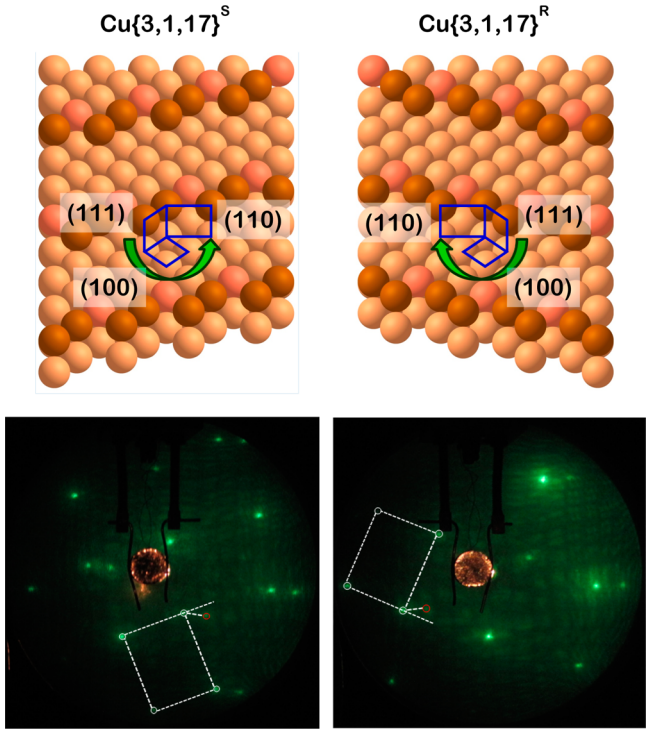

Figure 2. Upper panel. Ball model depiction of the ideal structures of the naturally chiral Cu{3,1,17}$^{R\&S}$ surfaces. The structures with clockwise and counterclockwise rotations among the three microfacets forming the terrace, step and kink, (111) → (100) → (110), are designated R and S, respectively. Lower panel. LEED patterns from clean Cu{3,1,17}$^{R\&S}$ single crystal surfaces (E = 225 eV, T = 90 K). The dashed lines highlight the repeating unit cell and the direction of the spot splitting due to the step edges. These are nonsuperimposable mirror images of one another, reflecting the chirality of the surfaces.

low symmetry directions and are, therefore, kinked and chiral. Close inspection of the LEED patterns reveals that the direction of the spot splitting is reversed on Cu{3,1,17}^{S} and Cu{3,1,17}^{R} images and that the LEED patterns are non-superimposable mirror images of one another. Thus, the LEED patterns of the clean Cu{3,1,17}^{S} and Cu{3,1,17}^{R} surfaces reveal the fact that their atomic surface structures are enantiomorphous and retain their surface chirality after sputtering and annealing under UHV conditions.

4.2. Enantiodifferentiation of Adsorbed D- and *L-Ala. Prior to probing the enantioselectivity of D*L-Ala adsorption on the Cu{3,1,17}$^{R\&S}$ surfaces, temperature-programmed reaction spectra (TPRS) were obtained from D-Ala/Cu{3,1,17}^{R}. During exposure to D-Ala, the surface was held at 440 K to prevent multilayer formation on the surface. After the surface was saturated with D-Ala, the sample was heated in front of the mass spectrometer at 1 K/s while monitoring the desorption signals at various mass-to-charge ratios. During heating, D-Ala/Cu{3,1,17}^{R} decomposed into several products and the species desorbing from the surface yielded prominent signals at m/q = 28, 41, and 44 in the mass spectrometer. While the identification of all decomposition products was not attempted for the purpose of this work, it is expected, by analogy with decomposition of other amino acids on Cu surfaces, that CO_2 (m/q = 44) is one of the major products.[29,61,62]

For the purpose of enantiodiscrimination of mixtures of the two enantiomers of Ala, we have used isotopically labeled *L-Ala ($HO_2{}^{13}C$ $CH(NH_2)CH_3$) and unlabeled D-Ala. TPR

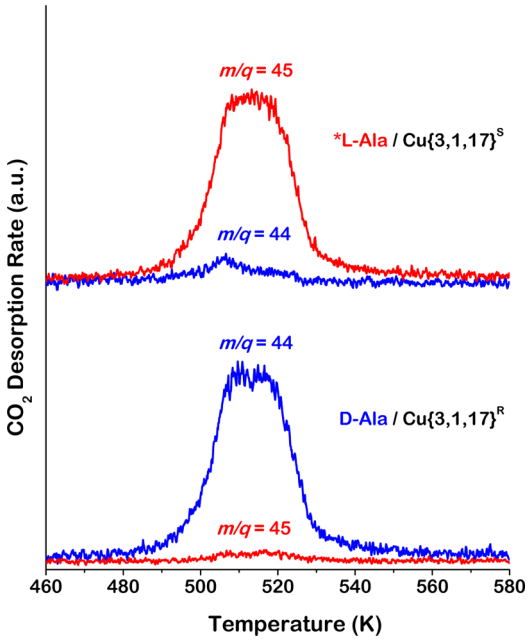

Figure 3. TPR spectra of D-Ala/Cu{3,1,17}^{R} and *L-Ala/Cu{3,1,17}^{S} at saturation coverage. *L-Ala/Cu{3,1,17}^{S} decomposition yields TPRS signal at m/q = 45, almost exclusively. D-Ala/Cu{3,1,17}^{R} decomposition yields TPRS signal at m/q = 44, almost exclusively. The yields of CO_2 and $^{13}CO_2$ can be used to estimate the coverages of D- and *L-Ala.

spectra of D-Ala/Cu{3,1,17}^{R} and *L-Ala/Cu{3,1,17}^{S} at saturation coverage are compared in Figure 3. Note that these two combinations are diastereomerically equivalent to one another and, as expected, the TPR spectra are identical, other than the fact that the product desorption signals appear at different masses as a result of isotopic labeled. During D-Ala decomposition the desorption signal at m/q = 44 is far greater than that at m/q = 45, while the signal at m/q = 45 dominates during *L-Ala decomposition. It is clear that the signals at m/q = 44 and 45 correspond to CO_2 and $^{13}CO_2$ desorption, respectively, and that they originate from the carboxylate groups of each Ala enantiomer. More importantly, the TPR spectra show that the signals at m/q = 44 from D-Ala and m/q = 45 from *L-Ala can be used for enantiodiscrimination and for measurement of the relative coverages of the two enantiomers on the surface. It is also important to note that the TPR spectra of all four combinations of D- and *L-Ala on the Cu{3,1,17}$^{R\&S}$ surfaces reveal no enantiospecificity to the decomposition kinetics (Figure 4). The peak temperatures and ranges for decomposition of D-Ala on Cu{3,1,17}$^{R\&S}$ are identical, as are the temperatures and ranges for *L-Ala on Cu{3,1,17}$^{R\&S}$. If the decomposition kinetics were enantiospecific, one would observe a temperature difference between the TPR spectra for D-Ala/Cu{3,1,17}^{R} and D-Ala/Cu{3,1,17}^{S} and likewise for *L-Ala/Cu{3,1,17}^{R} and *L-Ala/Cu{3,1,17}^{S}. This is readily observable in the decomposition of D- and L-tartaric acid on chiral Cu surfaces.[24]

As seen in Figure 3, the TPR spectra of *L-Ala and D-Ala reveal small signals at m/q = 44 and 45, respectively. These may arise from isotopic impurities or from other decomposition products. To account for these minority signals during analysis of TPR spectra from mixed layers of D-Ala and *L-Ala, the coverages of D- and *L-Ala were calculated by solving the equations

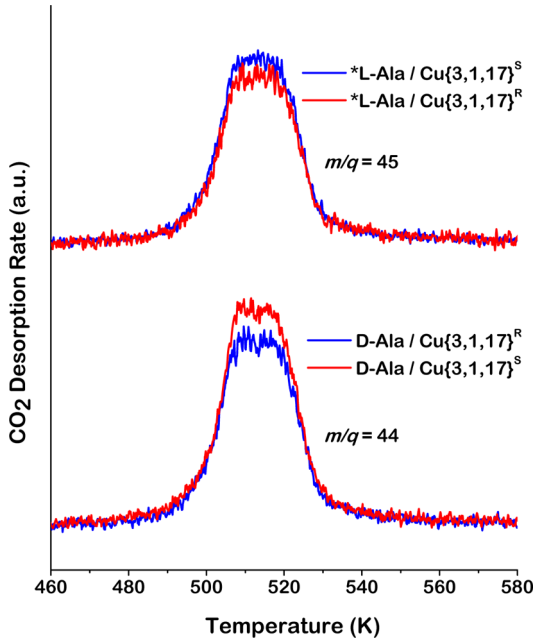

Figure 4. TPR spectra of D-Ala/Cu{3,1,17}$^{R\&S}$ and *L-Ala/Cu-{3,1,17}$^{R\&S}$ at saturation coverage. The peak decomposition temperatures and the decomposition temperature ranges for all four combinations of D-/*L-Ala on Cu{3,1,17}$^{R\&S}$ are indistinguishable. There is no measurable enantiospecificity in the Ala decomposition kinetics on Cu{3,1,17}$^{R\&S}$ surfaces.

$$Y_{44} = \alpha_{44}^{D}\theta_{D} + \alpha_{44}^{*L}\theta_{*L} \quad (1)$$

and

$$Y_{45} = \alpha_{45}^{D}\theta_{D} + \alpha_{45}^{*L}\theta_{*L}$$

where $Y_{m/q}$ are the integrated areas under TPRS peaks at each m/q ratio, α are the coefficients for D- and *L-Ala at each m/q ratio, and θ are the coverages of D- and *L-Ala. D- and *L-Ala yield signals at both m/q = 44 and 45 that are proportional to their coverages. The coefficients α_{44}^{D} and α_{45}^{D} (α_{44}^{*L} and α_{45}^{*L}) were obtained from the TPR spectra of pure D-Ala at $\theta_D = 1$ (pure *L-Ala at $\theta_{*L} = 1$). Using the system of eqs 1, the coverages of D- and *L-Ala were estimated from the integrated areas under the peaks at m/q = 44 and 45 measured from TPR spectra obtained after exposure to gas phase mixtures of the two enantiomers.

4.3. Equilibrium Adsorption of D*L-Ala on Cu-{3,1,17}$^{R\&S}$ surfaces. To study enantioselective adsorption of D*L-Ala, the Cu{3,1,17}$^{R\&S}$ surfaces at 440 K were exposed to racemic D*L-Ala for increasing periods of time. The partial pressure or flux ratio of $F_D/F_{*L} = 1$ was achieved by independently controlling the temperatures of the glass vials containing D-Ala and *L-Ala. Following exposure of the surfaces to the gas phase racemic mixture, the ratio of D-Ala/*L-Ala coverages, θ_D/θ_{*L}, was determined by TPRS as described above. Figure 5 shows a plot of the coverage ratio, $\ln(\theta_D/\theta_{*L})$, versus exposure time. The Cu{3,1,17}$^{R\&S}$ surfaces were saturated with Ala after ~10 min of exposure to the mixture. Following saturation of the surfaces, the ratio of the D- to *L-Ala coverages remains unity for exposure times up to 90 min, showing no enantioselective separation on either Cu{3,1,17}^{R} or Cu{3,1,17}^{S} surfaces.

To establish and measure equilibrium between racemic D*L-Ala in the gas phase and the D-Ala and *L-Ala adsorbed on the surface, it is necessary that D-Ala and *L-Ala displace one another rapidly on the time scale of the exposure. Mutual displacement of amino acid enantiomers was demonstrated in our prior study of D*L-Asp/Cu{3,1,17}$^{R\&S}$; however, the displacement rate is very sensitive to the surface temperature. Therefore, to determine whether the apparent adsorption equilibrium on the surfaces at 440 K was kinetically limited by low displacement rates, the Cu{3,1,17}^{R} surface was first prepared with a monolayer of Ala with $\theta_{D/R}/\theta_{*L/R}$ = 1.39 and then exposed to racemic D*L-Ala in the gas phase. Although the initial coverage ratio on the surface was $\theta_{D/R}/\theta_{*L/R} > 1$, continued exposure of the surface to the racemic D*L-Ala in the gas phase caused the coverage ratio to decrease and approach $\theta_{D/R}/\theta_{*L/R} = 1$ after ~60 min, (Figure 5, △). As an additional check, the Cu{3,1,17}^{R} surface was first prepared with a saturated layer of Ala with $\theta_{D/R}/\theta_{*L/R}$ = 0.58 and then exposed to racemic D*L-Ala. Although the initial coverage ratio on the surface was $\theta_{D/R}/\theta_{*L/R} < 1$, continued exposure of the surface to the racemic D*L-Ala in the gas phase caused the coverage ratio to increase and approach $\theta_{D/R}/\theta_{*L/R} = 1$ (Figure 5, ☆). These changes in $\theta_{D/R}/\theta_{*L/R}$ starting from both $\theta_{D/R}/\theta_{*L/R} < 1$ and > 1 and then approaching $\theta_{D/R}/\theta_{*L/R} = 1$ during exposure of the surface to racemic D*L-Ala confirm that the rate of displacement at 440 K between gas phase and adsorbed phase Ala is sufficient to achieve adsorption equilibrium of racemic D*L-Ala within the exposure time used. Hence, the equal coverages of D- and *L-Ala on the Cu{3,1,17}$^{R\&S}$ surfaces are the result of adsorption equilibrium with racemic mixtures of D- and *L-Ala in the gas phase.

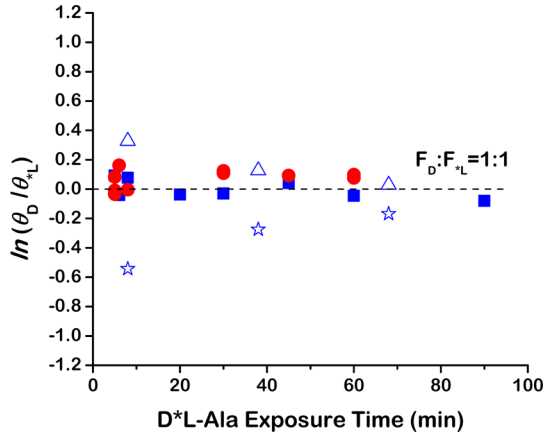

Figure 5. D- and *L-Ala coverage ratios, $\ln(\theta_D/\theta_{*L})$, on Cu{3,1,17}$^{R\&S}$ at 440 K as a function of exposure time to racemic D*L-Ala. During the exposure to clean Cu{3,1,17}^{R} (■) and Cu{3,1,17}^{S} (●) surfaces, θ_D/θ_{*L} = 1.0 for all exposure times, revealing no enantioselective separation. On the Cu{3,1,17}^{R} surface, the coverage ratio tends toward $\theta_D/\theta_{*L} \approx 1$ when starting with initial coverage ratios of 1.39 (△) or 0.58 (☆). This indicates that the equal coverages of the two enantiomers on the Cu{3,1,17}$^{R\&S}$ surfaces after long-term exposure are the result of equilibrium with the racemic mixture in the gas phase.

One of the key features of our experimental methodology is that we are able to expose the surfaces to gas phase D- and *L-Ala mixtures of arbitrary but controlled composition by individual control of the temperatures of the two evaporation sources. This ability is critical to understanding the nature of the equilibria being established between the gas phase and the adsorbed phase. For example, the fact that exposure of the Cu{3,1,17}$^{R\&S}$ surfaces to racemic D*L-Ala in the gas phase results in a racemic mixture $\theta_{D/R}/\theta_{*L/R} = 1$ on the surface could

result from the formation of a very energetically stable racemate phase on the surface, as suggested in Figure 1 in scenarios (DL)/R and (DL)/S. If that were the case, then the ratio of enantiomers in the adsorbed phase would be racemic and almost independent of the D-Ala/*L-Ala partial pressure ratio, P_D/P_{*L}, in the gas phase. Therefore, the equilibrium adsorption of D*L-Ala on the Cu{3,1,17}$^{R\&S}$ surfaces was also investigated during exposure to nonracemic D-/*L-Ala mixtures in the gas phase. The equilibrium D-/*L-Ala coverage ratios on Cu{3,1,17}$^{R\&S}$ surfaces for gas phase flux ratios of $F_D/F_{*L} = P_D/P_{*L} = 1/2$, 1, and 2 are shown in Figure 6. These clearly indicate

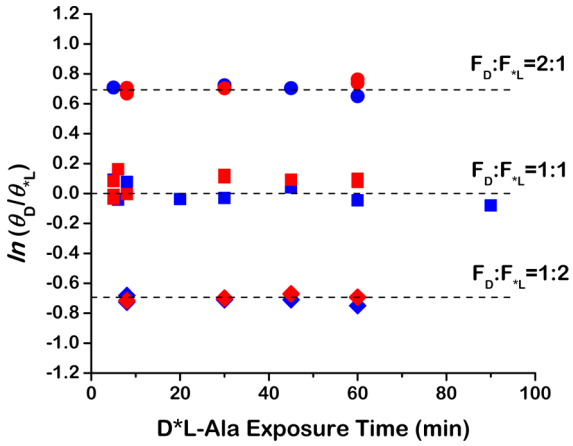

Figure 6. D-/*L-Ala coverage ratios, $\ln(\theta_D/\theta_{*L})$, on Cu{3,1,17}$^{R\&S}$ at 440 K as a function of exposure time to D-/*L-Ala gas mixtures with $P_D/P_{*L} = F_D/F_{*L} = 1/2$, 1, and 2. The ratios of adsorbed D- and *L-Ala on Cu{3,1,17}^{R} (blue symbols) and Cu{3,1,17}^{S} (red symbols) surfaces remain the same as the gas flux ratios, F_D/F_{*L}= 1/2, 1, and 2 for all exposure times. These results imply that D*L-Ala forms conglomerate phases of D- and *L-Ala with the same adsorption energies on the Cu{3,1,17}$^{R\&S}$ surfaces.

that the ratio of adsorbed species is dictated by the D-/*L-Ala partial pressure ratio in the gas phase; $\theta_D/\theta_{*L} = P_D/P_{*L}$ and is independent of the surface chirality.

4.4. DFT Calculations of D-, L-, and DL-Ala/Cu{3,1,17}^{S}.

The energetics of Ala adsorption on the Cu{3,1,17}^{S} surfaces have been calculated using DFT. These calculations have used the PW91 functional and the PBE-D2 functional that includes dispersion interactions. Preliminary calculations showed that PW91 and PBE did not produce significant changes to energy differences between the different dense adlayers. As outlined in section 3, the DFT calculations modeled the ideal Cu{3,1,17}$^{R\&S}$ unit cell with two deprotonated Ala molecules per unit cell. The configurations for each dense L-Ala adlayer and dense DL-Ala adlayer were generated from the four most favorable configurations found by Rankin and Sholl.[55] The configurations for dense D-Ala adlayers were then created by taking the earlier configurations and modifying the methyl group position as needed. Comparison of the PW91 and the PBE-D2 results can be found in Table 1 and the structures associated with these configurations are illustrated in the Supporting Information Figure SI1. Similar configurations were found to be most energetically stable using both the PW91 and the PBE-D2 functionals. These functionals also predicted roughly the same ordering of energies among higher energy configurations. This is consistent with the expectation that the total adsorption energy for these molecules is affected by dispersion contributions but that these contributions are

Table 1. Relative Energies[a] of Dense Alanine Adlayers on Cu{3,1,17}^{S}

dense adlayer PW91[55]	E (eV/unit cell)	dense adlayer PBE-D2	E (eV/unit cell)
L_1_0_a	0	L_1_0_a	0.00
DL_1_0_a	0.091	DL_1_0_a	−0.01
L_1_90_a	0.11	L_1_90_a	0.03
L_2_180_a	0.133	DL_2_180_a	0.22
DL_2_90_b	0.144	D_1_0_a	0.23
L_2_270_a	0.159	D_2_180_a	0.24
DL_1_90_b	0.198	L_2_180_a	0.25
DL_2_180_a	0.221	DL_2_90_b	0.28
L_4_270_b	0.235	DL_1_90_b	0.30
DL_2_270_a	0.256	L_2_270_a	0.30
DL_4_270_b	0.257	D_1_90_a	0.35
DL_1_90_a	0.274	D_1_90_b	0.37
L_1_90_b	0.303	D_2_90_b	0.39
L_2_90_b	0.402	D_2_270_a	0.40

[a]Relative energies are defined with respect to the L_1_0_a adlayer.

approximately equal for a large variety of adsorbate configurations at constant coverage. Since there were no significant changes to the ordering of energies among the configurations, it is unlikely that the other configurations examined by Rankin and Sholl would be more favorable than those already identified.[55]

These calculations effectively model the energetics of two conglomerate phases (D-Ala and L-Ala) and a racemate phase (DL-Ala). On the chiral Cu{3,1,17}$^{R\&S}$ surfaces, the adsorption energies of the conglomerate phases differ by $\Delta\Delta E_{DL} = \Delta E_{D/R} - \Delta E_{L/R} = \Delta E_{L/S} - \Delta E_{D/S}$. The adsorption energetics of the racemate phases are identical on the two surfaces, $\Delta E_{DL/R} = \Delta E_{DL/S}$, but they differ from the average energy of the conglomerate phases by $\Delta\Delta E_{r-c} = \Delta E_{DL/R} - {}^{1}/_{2}(\Delta E_{D/R} + \Delta E_{L/R})$. Figure 7 shows the most stable configurations of D-, L-,

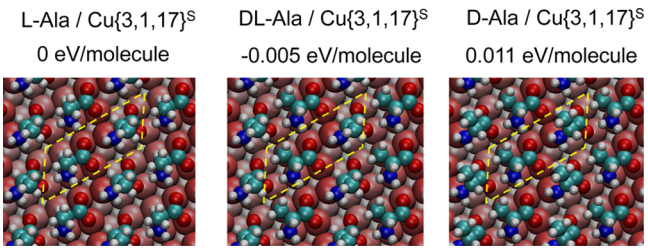

Figure 7. Structures and relative energies predicted using DFT-D2 for the most stable conformations of L-Ala, DL-Ala, and D-Ala on the Cu{3,1,17}^{S} surface. The energies are defined relative to the that of L-Ala/Cu{3,1,17}^{S}. The unit cell contains two adsorbed molecules. In the case of the racemic DL-Ala overlayer, the D-Ala enantiomer is adsorbed at the top of the step and extends onto the terrace, while the L-Ala enantiomer is adsorbed at the bottom of the step with the $-NH_2$ interacting with the least coordinated Cu atom in the step edge.

and DL-Ala on Cu{3,1,17}^{S} identified using DFT and the associated energies referenced to the most stable phase, L-Ala/Cu{3,1,17}^{S}. A key result of the DFT calculations is that they predict that the energetics of the conglomerate (D-Ala and L-Ala), and the racemate (DL-Ala) phases are comparable and thus, that both phases should be considered in describing adsorption of Ala from gas phase mixtures of enantiomers.

Inspection of the structures of the adsorbed overlayers of D- and L-Ala on the Cu{3,1,17}^{S} surface shows that there is a

single motif for the two molecules in each unit cell which is dictated by the binding of the $-CO_2$ and $-NH_2$ groups to the surface and is independent of chirality. The unit cells drawn into the structures shown in Figure 7 have been chosen to highlight the two Ala molecules within the unit cell. In all three structures, the Ala at the upper right of the unit cell is adsorbed at the bottom of the step edge with its $-CO_2$ group binding to two nearest neighbor Cu atoms in the Cu(100) terrace and its $-NH_2$ binding to the least coordinated Cu atom along the step edge. The Ala in the lower left of the unit cell in all three structures has its $-CO_2$ group binding to two nearest neighbor Cu atoms at the top of the step edge and its $-NH_2$ binding to a Cu atom in the Cu(100) terrace. The enantiospecific differences in the adsorption energetics of the two conglomerate phases and the racemate phase are dictated by stereospecific orientations of the $-H$ and $-CH_3$ groups on the C_α atom. The conglomerate L-Ala phase has the lower of the conglomerate phase energies and adopts a structure in which both of the $-CH_3$ groups are oriented away from the surface. The primary difference between the L-Ala phase and the racemic DL-Ala phase is that in the DL-Ala phase the molecule on the terrace (lower left) is reversed in chirality from L-Ala to D-Ala and it now has its $-CH_3$ interacting with the Cu(100) terrace. The DL-Ala phase is very slightly more stable (−0.005 eV/molecule) than the L-Ala phase. On switching from the DL-Ala phase to the D-Ala phase it is the chirality of the molecule at the bottom of the step edge (upper right) that is reversed, forcing the $-CH_3$ to interact with the step edge. This has a much larger impact on the adsorption energy than reorientation of the $-CH_3$ group in the Ala on the terrace and destabilizes the D-Ala phase with respect to the L-Ala and the DL-Ala phases by ∼0.11 eV/molecule.

DFT predicts a number of common structural features of the conglomerate and racemate phases of D- and L-Ala on Cu{3,1,17}^{S} that are invariant under reversal of the chirality of C_α in the amino acid. However, it also predicts that the subtle differences in structure induced by the reversal of the chirality are accompanied by adsorption energy differences of ∼0.11 eV/molecule. As we will discuss below, these energy predictions are at odds with our experimental observations.

5. DISCUSSION

5.1. Self-Displacement of Amino Acids on Cu Surfaces. A critical element of the experimental protocol for measurement of the equilibrium adsorption of enantiomer mixtures is that a steady state flux from the gas phase can displace the adsorbed enantiomers on the experimental time scale; in this case ∼60 min. This has been demonstrated in the case of Ala on Cu{3,1,17}$^{R\&S}$ as illustrated in Figure 5, and in the case of Asp on Cu{3,1,17}$^{R\&S}$.[29] The fact that gas phase species can displace strongly adsorbed species under UHV conditions was first demonstrated by Madix et al. on Cu and Ag and used to rank the relative acidities of various different adsorbates based on their ability to displace one another.[63,64] The displacement phenomenon was first used by Gellman et al. for quantitative measurement of adsorption equilibria using partially fluorinated alkoxides on Cu surfaces.[65,66] The fact that amino acids and their enantiomers can displace one another from Cu{3,1,17}$^{R\&S}$ surfaces is entirely consistent with these previous observations.

The mechanism of the amino acid displacement process is an interesting problem in its own right and is not completely understood, although our observations shed some light. Alanine adsorbs on Cu surfaces in a deprotonated form as an alaninate that decomposes during heating rather than desorbing from the surface.[30−40] Under UHV conditions, the temperatures used for the displacement experiment are too low for significant decomposition of alaninate on the experimental time scale. Nonetheless, in the presence of a gas phase flux of D-alanine, *L-alaninate is displaced from the surface. The mechanism is believed to be one in which transiently adsorbed D-alanine undergoes proton transfer to *L-alaninate creating *L-alanine that then desorbs, leaving D-alaninate adsorbed to the surface.

5.2. Enantiospecific Energies of D*L-Ala Phases on Cu{3,1,17}$^{R\&S}$ Surfaces. If one can model the coadsorption of two enantiomers onto a chiral surface as a first-order, competitive Langmuir adsorption process, then measurements of adsorption isotherms, $\theta_D(P_D, P_L)|_T$ and $\theta_L(P_D, P_L)|_T$, on chiral surfaces such as Cu{3,1,17}$^{R\&S}$ can be used to determine the ratio of adsorption equilibrium constants and, therefore, the enantiospecific difference in adsorption free energies.[29]

$$\frac{\theta_{D/R}}{\theta_{L/R}} = \frac{K_{D/R}P_D}{K_{L/R}P_L} = \frac{K_{L/S}P_L}{K_{D/S}P_D} = \frac{\theta_{L/S}}{\theta_{D/S}}$$

This has been used successfully to model the competitive, enantiospecific coadsorption of D- and *L-Asp on the Cu{3,1,17}$^{R\&S}$ surfaces. In that case, exposure of the Cu{3,1,17}$^{R\&S}$ surfaces to racemic D*L-Asp in the gas phase resulted in coverages on the surfaces that deviated from unity; $\theta_{D/R}/\theta_{*L/R}$ = 0.46 on Cu{3,1,17}^{R} and $\theta_{D/S}/\theta_{*L/S}$ = 2.30 on Cu{3,1,17}^{S}. These were then used to estimate the ratio of the enantiospecific equilibrium constants for adsorption of D- and *L-Asp on Cu{3,1,17}^{S}. Additional experiments using nonracemic mixtures with gas phase partial pressure ratios of P_D/P_{*L} = $^1/_2$ and 2 yielded the same values for the ratio of the equilibrium constants; $K_{D/S}/K_{D/R}$ = 2.29 ± 0.17. The ratio of the equilibrium constants is independent of the relative D- and *L-Asp coverages.

Similar to crystallization of chiral mixtures in 3D, mixtures of D- and L-enantiomers can, in principle, form three distinct phases during 2D crystallization on surfaces: two enantiomorphous conglomerate phases (D- or L-) and a racemic compound (DL-).[31,67−70] The DFT energetics calculated in the course of this work (Figure 7) suggest that all three adsorbed phases ought to be considered. If the racemate DL-phase were far more energetically stable than either the D- or the L- phase, as indicated in Figure 1 scenarios (DL)/R and (DL)/S, then the equilibrium ratio of the enantiomers on Cu{3,1,17}$^{R\&S}$ would be $\theta_{D/R}/\theta_{*L/R} = \theta_{*L/S}/\theta_{D/S}$ = 1 and insensitive to the ratio of the partial pressures of the enantiomers in the gas phase, P_D/P_{*L}. The data in Figure 6 demonstrates that this is clearly not the case for D- and *L-Asp adsorption on Cu{3,1,17}$^{R\&S}$.

The coadsorption of D- and L-Ala on the Cu{3,1,17}$^{R\&S}$ surfaces is fundamentally different from that of D- and L-Asp. As shown in Figure 6, the ratio of D- to *L-Ala coverages on the Cu{3,1,17}$^{R\&S}$ surfaces remained $\theta_{D/R}/\theta_{*L/R} = \theta_{*L/S}/\theta_{D/S}$ = 1 during exposure to racemic D*L-Ala for all exposure times. One explanation for the fact that the coverage ratio does not deviate from unity and is identical on both enantiomorphous surfaces is that D- and *L-Ala do not interact enantiospecifically with the Cu{3,1,17}$^{R\&S}$ surfaces, $\Delta\Delta E_{DL}$ = 0. The other possible explanation is the formation of a racemic D*L-Ala phase which is much more energetically stable than either of the conglomerate phases. If that were the case, exposure to nonracemic mixtures of D- and *L-Ala in the gas phase, P_D/P_{*L}

$\neq 1$, would lead to a coverage ratio on the surfaces of $\theta_{D/R}/\theta_{*L/R} = \theta_{*L/S}/\theta_{D/S} = 1$. However, it is quite clear from the data in Figure 6 that $\theta_{D/R}/\theta_{*L/R} = \theta_{D/S}/\theta_{*L/S} = P_D/P_{*L}$. These results point quite clearly to the scenario in which the adsorption of D- and *L-Ala on the Cu{3,1,17}$^{R\&S}$ surfaces is not measurably enantiospecific, $\Delta\Delta E_{D*L} = 0$, and that the racemate D*L-Ala phase is energetically unstable with respect to the conglomerate D- and *L-Ala phases. It is important to note that, although we refer to the stable phases as conglomerate phases as though they are enantiomerically pure 2D domains (Figure 1), the extent of these domains could vary from isolated molecules to extended islands. In other words, the data are also consistent with a random 2D solution of noninteracting D- and L-Ala on the surface, but not with the formation of DL-Ala dimers or extended racemate domains.

To our knowledge, the only available experimental data relevant to the enantiospecific adsorption energetics of Ala on Cu{3,1,17}$^{R\&S}$ surfaces come from STM images of L-Ala/Cu(100).[71] The adsorption of L-Ala on Cu(100) surfaces induces step bunching resulting in the formation of {3,1,17} facets. This has also been observed in the case of glycine and L-lysine adsorption on Cu(100).[33,72] There are eight {3,1,17} facets vicinal to the (100) plane, four {3,1,17}^{R} and four {3,1,17}^{S} facets. In the case of faceting induced by L-lysine adsorption on Cu(100), only the four {3,1,17}^{R} facets are observed.[72] A TPD study of D- and L-lysine desorption from Cu(100) and Cu{3,1,17}$^{R\&S}$ surfaces showed that the adsorption energies of D- and L-lysine on Cu(100) were lower than on the Cu{3,1,17}$^{R\&S}$ surfaces, hence the driving force for faceting.[21] More importantly, the adsorption energies of L-lysine/Cu{3,1,17}^{R} and D-lysine/Cu{3,1,17}^{S} were lower than the adsorption energies of D-lysine/Cu{3,1,17}^{R} and L-lysine/Cu{3,1,17}^{S}, hence the driving force for the preferential formation of the {3,1,17}^{R} facets during the adsorption of L-lysine on Cu(100). In contrast with the adsorption of L-lysine on Cu(100), the surface reconstruction induced by glycine, an achiral amino acid, on Cu(100) results in a roughly equal numbers of {3,1,17}^{R} and {3,1,17}^{S} facets. This result for glycine is not surprising because it is achiral and, therefore, cannot interact enantiospecifically with the Cu{3,1,17}$^{R\&S}$ facets. As in the case of glycine, the surface reconstruction induced by L-Ala on Cu(100) results in roughly equal numbers of {3,1,17}^{R} and {3,1,17}^{S} facets.[71] By analogy with glycine/Cu(100) and in contrast to L-lysine/Cu(100), this result for L-Ala/Cu(100) suggests that L-Ala does not interact enantiospecifically with Cu{3,1,17}$^{R\&S}$ surfaces. This is consistent with the direct observations of D-/*L-Ala adsorption on Cu{3,1,17}$^{R\&S}$ surfaces made in this work.

5.3. Relative Adsorption Energetics from Experiment and DFT. The structures of D-, L- and DL-Ala monolayers on Cu{3,1,17}$^{R\&S}$ surfaces predicted by DFT and illustrated in Figure 7 have one of the two molecules within each unit cell adsorbed on the (100) terrace and the other at the lower edge of the kinked step. There are also common features associated with the binding sites of the $-CO_2$ and the $-NH_2$ groups of the two molecules in each of the most stable configurations of the three monolayers. The differences between the three structures can be readily associated with the orientations of the $-CH_3$ and the $-H$ in each enantiomer. Switching the chirality of the molecule adsorbed on the (100) terrace (Figure 7, lower left in the unit cell) makes little difference to the adsorption energy, consistent with this being an "achiral" binding site. However, switching the chirality of the molecule adsorbed at the lower edge of the step (Figure 7, upper right in the unit cell) has a significant impact on the binding energy, consistent with this being the chiral binding site.

The obvious inconsistency in the work presented is that while the DFT calculations predict an enantiospecific interaction of D- and L-Ala with the Cu{3,1,17}$^{R\&S}$ surfaces, the experimental results reveal none. One of the values of the DFT calculations is that they have revealed the possibility that the D-, L-, and DL-Ala phases on Cu{3,1,17}^{S} can have comparable energies and thus, that the contribution of a DL-Ala phase should be considered in our analysis of the adsorption equilibria. Fortunately, our experimental method is capable of measuring equilibria between adsorbed phases and gas phase mixtures of arbitrary composition. This allows us to discriminate between the two mechanisms by which exposure to a gaseous racemic mixture might lead to adsorption of a racemic mixture on the surface: the scenario in which the racemic DL-Ala phase is far more stable than either D- or L-Ala (Figure 1, scenarios (DL)/R and (DL)/S), and the scenario in which the energies of the D- and L-Ala phases are indistinguishable (Figure 1, scenarios (D + L)/R and (D + L)/S). The latter with $\Delta\Delta E_{DL} \approx 0$ is consistent with the experimental results.

It is worthwhile addressing the question of why the DFT and experimental results differ. One possibility is that the enantiospecific and configuration specific energy differences between the D-, L-, and DL-Ala phases on the Cu{3,1,17}$^{R\&S}$ surfaces are simply too small to be resolved by DFT, even when using a dispersion corrected functional. If one examines the enantiospecificities of reaction rates, desorption energetics and adsorption equilibria measure on well-defined, naturally chiral single crystal surfaces,[14,21,24,29] the highest enantiospecific difference in reaction energetics that one would estimate from those measurements is ~0.04 eV/molecule estimated for the desorption of methyl lactate from Cu{643}^{R}.[73] This value is probably at the limit of what can be reliably achieved using DFT.[74] That being the case, prediction of enantioselectivities from computational modeling remains a challenge.

As with all attempts to compare the predictions of computational simulation with the results of experimental measurement, success relies not only on the accuracy of the simulation method, but equally on the fidelity of the model of the physical reality being measured. The discrepancy between the predictions of DFT and the experimental results could arise simply from an incorrect description of Ala on Cu{3,1,17}^{S}. The experimental measurements were performed on thermally roughened surfaces that were saturated with adsorbed Ala, but at an absolute coverage that has not been determined quantitatively. The DFT model assumes that the surface exposes an ideal Cu{3,1,17}^{S} unit cell with two Ala molecules per unit cell adsorbed in deprotonated states. We cannot exclude the possibility that this coverage does not match that of the experiment exactly. Perhaps the species being modeled is not that adsorbed on the real surface. Several studies suggest that adsorbed acids, including amino acids and tartaric acid, can extract Cu atoms from the surface to form adsorbed species that are better described as Cu salts than adsorbed carboxylates.[72,75−78] It is conceivable that the species on the surface is a Cu-alaninate and the surface structure is quite different from the ideal Cu{3,1,17}^{S}. The discrepancy between our experimental results and our DFT based simulation is not entirely surprising given the subtlety of the phenomena that we are studying. Converging to a fully consistent picture of the

enantioselective adsorption of Ala on Cu{3,1,17}$^{R\&S}$ poses a challenge to both the computational methods being used, and to the experimental characterization of the system under study.

6. CONCLUSIONS

The equilibrium adsorption of mixtures of isotopically labeled *L-Ala and unlabeled D-Ala with variable partial pressure ratios, P_D/P_{*L}, allows discrimination between adsorption as D- and *L-conglomerate phases and adsorption in a DL-racemate phase. D- and *L-Ala adsorb on the Cu{3,1,17}$^{R\&S}$ surfaces in conglomerate phases but with adsorption energetics that are not measurably enantiospecific.

■ ASSOCIATED CONTENT

Supporting Information

Figure SI1 which shows the atomistic structures of the D-/L-/DL-alanine overlayer configurations listed in Table 1. This material is available free of charge via the Internet at http://pubs.acs.org.

■ AUTHOR INFORMATION

Corresponding Author

*E-mail: gellman@cmu.edu.

Notes

The authors declare no competing financial interest.

■ ACKNOWLEDGMENTS

D.S.S. acknowledges support for the DFT study from NSF CHE-1012524. A.J.G. acknowledges support for the experimental component of the study from the US DOE through Grant No. DE-FG02-12ER16330.

■ REFERENCES

(1) Bonner, W. A. The Origin and Amplification of Biomolecular Chirality. *Origins Life Evol. Biosphere* **1991**, *21* (2), 59−111.

(2) Bada, J. L. Biomolecules—Origins of Homochirality. *Nature* **1995**, *374* (6523), 594−595.

(3) Merino, I. M.; Gonzalez, E. B.; Sanzmedel, A. Liquid-Chromatographic Separation of Penicillamine Enantiomers Derivatized with Opa/2-Me on a Beta-Cyclodextrin Bonded Phase. *Mikrochim. Acta* **1992**, *107* (1−2), 73−80.

(4) Sholl, D. S.; Gellman, A. J. Developing Chiral Surfaces for Enantioselective Chemical Processing. *AlChE J.* **2009**, *55* (10), 2484−2490.

(5) Smith, S. W. Chiral Toxicology: It's the Same Thing...Only Different. *Toxicol. Sci.* **2009**, *110* (1), 4−30.

(6) Erb, S. Single-Enantiomer Drugs Poised for Further Market Growth. *Pharm. Technol.* **2006**, *30*, s14−s18.

(7) Baddeley, C. J. Fundamental Investigations of Enantioselective Heterogeneous Catalysis. *Top. Catal.* **2003**, *25* (1−4), 17−28.

(8) Lorenzo, M. O.; Baddeley, C. J.; Muryn, C.; Raval, R. Extended Surface Chirality from Supramolecular Assemblies of Adsorbed Chiral Molecules. *Nature* **2000**, *404* (6776), 376−379.

(9) Barlow, S. M.; Raval, R. Complex Organic Molecules at Metal Surfaces: Bonding, Organisation and Chirality. *Surf. Sci. Rep.* **2003**, *50* (6−8), 201−341.

(10) Parschau, M.; Romer, S.; Ernst, K. H. Induction of Homochirality in Achiral Enantiomorphous Monolayers. *J. Am. Chem. Soc.* **2004**, *126* (47), 15398−15399.

(11) McFadden, C. F.; Cremer, P. S.; Gellman, A. J. Adsorption of Chiral Alcohols on "Chiral" Metal Surfaces. *Langmuir* **1996**, *12* (10), 2483−2487.

(12) Gellman, A. J. Chiral Surfaces: Accomplishments and Challenges. *ACS Nano* **2010**, *4* (1), 5−10.

(13) Baber, A. E.; Gellman, A. J.; Sholl, D. S.; Sykes, E. C. H. The Real Structure of Naturally Chiral Cu{643}. *J. Phys. Chem. C* **2008**, *112* (30), 11086−11089.

(14) Horvath, J. D.; Gellman, A. J. Enantiospecific Desorption of Chiral Compounds from Chiral Cu(643) and Achiral Cu(111) Surfaces. *J. Am. Chem. Soc.* **2002**, *124* (10), 2384−2392.

(15) Horvath, J. D.; Koritnik, A.; Kamakoti, P.; Sholl, D. S.; Gellman, A. J. Enantioselective Separation on a Naturally Chiral Surface. *J. Am. Chem. Soc.* **2004**, *126* (45), 14988−14994.

(16) Kuhnle, A.; Linderoth, T. R.; Besenbacher, F. Enantiospecific Adsorption of Cysteine at Chiral Kink Sites on Au(110)-(1 × 2). *J. Am. Chem. Soc.* **2006**, *128* (4), 1076−1077.

(17) Eralp, T.; Ievins, A.; Shavorskiy, A.; Jenkins, S. J.; Held, G. The Importance of Attractive Three-Point Interaction in Enantioselective Surface Chemistry: Stereospecific Adsorption of Serine on the Intrinsically Chiral Cu{531} Surface. *J. Am. Chem. Soc.* **2012**, *134* (23), 9615−21.

(18) Held, G.; Gladys, M. J. The Chemistry of Intrinsically Chiral Surfaces. *Top. Catal.* **2008**, *48* (1−4), 128−136.

(19) Schillinger, R.; Šljivančanin, Ž.; Hammer, B.; Greber, T., Probing Enantioselectivity with X-ray Photoelectron Spectroscopy and Density Functional Theory. *Phys. Rev. Lett.* **2007**, *98* (13).

(20) Horvath, J. D.; Gellman, A. J. Enantiospecific Desorption of R- and S-Propylene Oxide from a Chiral Cu(643) Surface. *J. Am. Chem. Soc.* **2001**, *123* (32), 7953−7954.

(21) Cheong, W. Y.; Gellman, A. J. Energetics of Chiral Imprinting of Cu(100) by Lysine. *J. Phys. Chem. C* **2011**, *115* (4), 1031−1035.

(22) Huang, Y.; Gellman, A. J. Enantiospecific Adsorption of (*R*)-3-Methylcyclohexanone on Naturally Chiral Surfaces Vicinal to Cu(110). *Top. Catal.* **2011**, *54* (19−20), 1403−1413.

(23) Rampulla, D. M.; Francis, A. J.; Knight, K. S.; Gellman, A. J. Enantioselective Surface Chemistry of *R*-2-Bromobutane on Cu(643)-(R&S) and Cu(531)(R&S). *J. Phys. Chem. B* **2006**, *110* (21), 10411−10420.

(24) Gellman, A. J.; Huang, Y.; Feng, X.; Pushkarev, V. V.; Holsclaw, B.; Mhatre, B. S. Superenantioselective Chiral Surface Explosions. *J. Am. Chem. Soc.* **2013**, *135* (51), 19208−19214.

(25) Horvath, J. D.; Baker, L.; Gellman, A. J. Enantiospecific Orientation of *R*-3-Methylcyclohexanone on the Chiral Cu(643)(R/S) Surfaces. *J. Phys. Chem. C* **2008**, *112* (20), 7637−7643.

(26) Gladys, M. J.; Stevens, A. V.; Scott, N. R.; Jones, G.; Batchelor, D.; Held, G. Enantiospecific Adsorption of Alanine on the Chiral Cu{531} Surface. *J. Phys. Chem. C* **2007**, *111* (23), 8331−8336.

(27) Attard, G. A.; Ahmadi, A.; Feliu, J.; Rodes, A.; Herrero, E.; Blais, S.; Jerkiewicz, G. Temperature Effects in the Enantiomeric Electro-Oxidation of D- and L-Glucose on Pt{643}(S). *J. Phys. Chem. B* **1999**, *103* (9), 1381−1385.

(28) Attard, G. A. Electrochemical Studies of Enantioselectivity at Chiral Metal Surfaces. *J. Phys. Chem. B* **2001**, *105* (16), 3158−3167.

(29) Yun, Y.; Gellman, A. J. Enantioselective Separation on Naturally Chiral Metal Surfaces: D,L-Aspartic Acid on Cu(3,1,17)(R&S) Surfaces. *Angew. Chem., Int. Ed.* **2013**, *52* (12), 3394−3397.

(30) Williams, J.; Haq, S.; Raval, R. The Bonding and Orientation of the Amino Acid L-Alanine on Cu{110} Determined by Rairs. *Surf. Sci.* **1996**, *368*, 303−309.

(31) Haq, S.; Massey, A.; Moslemzadeh, N.; Robin, A.; Barlow, S. M.; Raval, R. Racemic versus Enantiopure Alanine on Cu(110): An Experimental Study. *Langmuir* **2007**, *23* (21), 10694−10700.

(32) Iwai, H.; Egawa, C. Molecular Orientation and Intermolecular Interaction in Alanine on Cu(001). *Langmuir* **2010**, *26* (4), 2294−300.

(33) Zhao, X. Y.; Gai, Z.; Zhao, R. G.; Yang, W. S.; Sakurai, T. Adsorption of Glycine on Cu(001) and Related Step Faceting and Bunching. *Surf. Sci.* **1999**, *424* (2−3), L347−L351.

(34) Efstathiou, V.; Woodruff, D. P. Characterisation of the Interaction of Glycine with Cu(100) and Cu(111). *Surf. Sci.* **2003**, *531* (3), 304−318.

(35) Sayago, D. I.; Polcik, M.; Nisbet, G.; Lamont, C. L. A.; Woodruff, D. P. Local Structure Determination of a Chiral Adsorbate: Alanine on Cu(110). *Surf. Sci.* **2005**, *590* (1), 76−87.

(36) Zhao, X.; Zhao, R.; Yang, W. Adsorption of Alanine on Cu(001) Studied by Scanning Tunneling Microscopy. *Surf. Sci.* **1999**, *442*, L995−L1000.
(37) Sayago, D.; Polcik, M.; Nisbet, G.; Lamont, C.; Woodruff, D. Local Structure Determination of a Chiral Adsorbate: Alanine on Cu(110). *Surf. Sci.* **2005**, *590* (1), 76−87.
(38) Barlow, S.; Louafi, S.; Leroux, D.; Williams, J.; Muryn, C.; Haq, S.; Raval, R. Polymorphism in Supramolecular Chiral Structures of R- and S-Alanine on Cu(110). *Surf. Sci.* **2005**, *590* (2−3), 243−263.
(39) Ge, S.; Lu, C.; Zhao, R. Adsorption of L-Alanine on Cu(111) Studied by Scanning Tunnelling Microscopy. *Chin. Phys. Lett.* **2006**, *23* (6), 1558−1561.
(40) Iwai, H.; Egawa, C. Molecular Orientation and Intermolecular Interaction in Alanine on Cu(001). *Langmuir* **2010**, *26* (4), 2294−2300.
(41) Clegg, M. L.; Morales de la Garza, L.; Karakatsani, S.; King, D. A.; Driver, S. M. Chirality in Amino Acid Overlayers on Cu Surfaces. *Top. Catal.* **2011**, *54* (19−20), 1429−1444.
(42) Rankin, R. B.; Sholl, D. S. Structures of Dense Glycine and Alanine Adlayers on Chiral Cu(3,1,17) Surfaces. *Langmuir* **2006**, *22* (19), 8096−8103.
(43) Rankin, R. B.; Sholl, D. S. First-Principles Studies of Chiral Step Reconstructions of Cu(100) by Adsorbed Glycine and Alanine. *J. Chem. Phys.* **2006**, *124* (7), 74703.
(44) Jacques, J.; Collet, A.; Wilen, S. H. *Enantiomers, Racemates, and Resolutions*; Wiley: New York, 1981; p xv.
(45) Klussmann, M.; Iwamura, H.; Mathew, S. P.; Wells, D. H.; Pandya, U.; Armstrong, A.; Blackmond, D. G. Thermodynamic Control of Asymmetric Amplification in Amino Acid Catalysis. *Nature* **2006**, *441* (7093), 621−623.
(46) Kresse, G.; Hafner, J. Ab Initio Molecular-Dynamics for Liquid-Metals. *Phys. Rev. B* **1993**, *47* (1), 558−561.
(47) Kresse, G.; Hafner, J. Ab-Initio Molecular-Dynamics Simulation of the Liquid-Metal Amorphous-Semiconductor Transition in Germanium. *Phys. Rev. B* **1994**, *49* (20), 14251−14269.
(48) Kresse, G.; Furthmuller, J. Efficiency of ab-Initio Total Energy Calculations for Metals and Semiconductors Using a Plane-Wave Basis Set. *Comput. Mater. Sci.* **1996**, *6* (1), 15−50.
(49) Kresse, G.; Furthmuller, J. Efficient Iterative Schemes for ab Initio Total-Energy Calculations Using a Plane-Wave Basis Set. *Phys. Rev. B* **1996**, *54* (16), 11169−11186.
(50) Perdew, J. P.; Burke, K.; Wang, Y. Generalized Gradient Approximation for the Exchange-Correlation Hole of a Many-Electron System. *Phys. Rev. B* **1996**, *54* (23), 16533−16539.
(51) Perdew, J. P.; Burke, K.; Ernzerhof, M. Generalized Gradient Approximation Made Simple (Vol 77, Pg 3865, 1996). *Phys. Rev. Lett.* **1997**, *78* (7), 1396−1396.
(52) Blochl, P. E. Projector Augmented-Wave Method. *Phys. Rev. B* **1994**, *50* (24), 17953−17979.
(53) Kresse, G.; Joubert, D. From Ultrasoft Pseudopotentials to the Projector Augmented-Wave Method. *Phys. Rev. B* **1999**, *59* (3), 1758−1775.
(54) Grimme, S. Semiempirical Gga-Type Density Functional Constructed with a Long-Range Dispersion Correction. *J. Comput. Chem.* **2006**, *27* (15), 1787−1799.
(55) Rankin, R.; Sholl, D. Structure of Dense Glycine and Alanine Adlayers on Chiral Cu(3,1,17) Surface. *Langmuir* **2006**, *22* (19), 8096−8103.
(56) Sholl, D. S.; Asthagiri, A.; Power, T. D. Naturally Chiral Metal Surfaces as Enantiospecific Adsorbents. *J. Phys. Chem. B* **2001**, *105* (21), 4771−4782.
(57) Power, T. D.; Asthagiri, A.; Sholl, D. S. Atomically Detailed Models of the Effect of Thermal Roughening on the Enantiospecificity of Naturally Chiral Platinum Surfaces. *Langmuir* **2002**, *18* (9), 3737−3748.
(58) Asthagiri, A.; Feibelman, P. J.; Sholl, D. S. Thermal Fluctuations in the Structure of Naturally Chiral Pt Surfaces. *Top. Catal.* **2002**, *18* (3−4), 193−200.
(59) Clegg, M. L.; Driver, S. M.; Blanco-Rey, M.; King, D. A. Atomic Roughness of an Intrinsically Chiral Surface Orientation of an fcc Metal: Cu{531}. *J. Phys. Chem. C* **2010**, *114* (9), 4114−4117.
(60) Ertl, G.; Küppers, J. *Low Energy Electrons and Surface Chemistry*, 2nd, completely rev. ed.; VCH: Weinheim; Deerfield Beach, FL, 1985; p xii.
(61) Eralp, T.; Cornish, A.; Shavorskiy, A.; Held, G. The Study of Chiral Adsorption Systems Using Synchrotron-Based Structural and Spectroscopic Techniques: Stereospecific Adsorption of Serine on Au-Modified Chiral Cu{531} Surfaces. *Top. Catal.* **2011**, *54* (19−20), 1414−1428.
(62) Roth, C.; Ernst, K. H. Surface Explosion Chemistry of Malic Acid on Cu(110). *Top. Catal.* **2011**, *54* (19−20), 1378−1383.
(63) Barteau, M. A.; Madix, R. J. A Study of the Relative Bronsted Acidities of Surface Complexes on Ag(110). *Surf. Sci.* **1982**, *120* (2), 262−272.
(64) Jorgensen, S. W.; Madix, R. J. The Relative Acidities of Gas-Phase Acids for Displacement of Surface Intermediates. *Surf. Sci.* **1983**, *130* (1), L291−L293.
(65) Dai, Q.; Gellman, A. J. Fluorine Substituent Effects on Alkoxide Chemistry and Orientation on the Cu(100) Surface. *J. Phys. Chem.* **1993**, *97* (41), 10783−10789.
(66) Gellman, A. J.; Dai, Q. Mechanism of β-Hydride Elimination in Adsorbed Alkoxides. *J. Am. Chem. Soc.* **1993**, *115* (2), 714−722.
(67) Eralp, T.; Shavorskiy, A.; Zheleva, Z. V.; Held, G.; Kalashnyk, N.; Ning, Y.; Linderoth, T. R. Global and Local Expression of Chirality in Serine on the Cu{110} Surface. *Langmuir* **2010**, *26* (24), 18841−51.
(68) Kuhnle, A.; Linderoth, T. R.; Hammer, B.; Besenbacher, F. Chiral Recognition in Dimerization of Adsorbed Cysteine Observed by Scanning Tunnelling Microscopy. *Nature* **2002**, *415* (6874), 891−893.
(69) Santagata, N. M.; Lakhani, A. M.; Davis, B. F.; Luo, P. S.; Nardelli, M. B.; Pearl, T. P. Chiral Steering of Molecular Organization in the Limit of Weak Adsorbate-Substrate Interactions: Enantiopure and Racemic Tartaric Acid Domains on Ag(111). *J. Phys. Chem. C* **2010**, *114* (19), 8917−8925.
(70) Romer, S.; Behzadi, B.; Fasel, R.; Ernst, K. H. Homochiral Conglomerates and Racemic Crystals in Two Dimensions: Tartaric Acid on Cu(110). *Chem.—Eur. J.* **2005**, *11* (14), 4149−4154.
(71) Zhao, X. Y.; Zhao, R. G.; Yang, W. S. Adsorption of Alanine on Cu(001) Studied by Scanning Tunneling Microscopy. *Surf. Sci.* **1999**, *442* (2), L995−L1000.
(72) Zhao, X. Y.; Zhao, R. G.; Yang, W. S. Scanning Tunneling Microscopy Investigation of L-Lysine Adsorbed on Cu(001). *Langmuir* **2000**, *16* (25), 9812−9818.
(73) Fleming, C.; King, M.; Kadodwala, M. Highly Efficient Electron Beam Induced Enantioselective Surface Chemistry. *J. Phys. Chem. C* **2008**, *112* (47), 18299−18302.
(74) Sholl, D. S.; Steckel, J. A. *Density Functional Theory: A Practical Introduction*; Wiley: New York, 2009.
(75) Roth, C.; Parschau, M.; Ernst, K. H. Chiral Reconstruction of a Metal Surface by Adsorption of Racemic Malic Acid. *ChemPhysChem* **2011**, *12* (8), 1572−1577.
(76) Roth, C.; Passerone, D.; Merz, L.; Parschau, M.; Ernst, K. H. Two-Dimensional Self-Assembly of Chiral Malic Acid on Cu(110). *J. Phys. Chem. C* **2011**, *115* (4), 1240−1247.
(77) Mhatre, B. S.; Pushkarev, V.; Holsclaw, B.; Lawton, T. J.; Sykes, E. C. H.; Gellman, A. J. A Window on Surface Explosions: Tartaric Acid on Cu(110). *J. Phys. Chem. C* **2013**, *117* (15), 7577−7588.
(78) Lawton, T. J.; Pushkarev, V.; Wei, D.; Lucci, F. R.; Sholl, D. S.; Gellman, A. J.; Sykes, E. C. H. Long Range Chiral Imprinting of Cu(110) by Tartaric Acid. *J. Phys. Chem. C* **2013**, *117* (43), 22290−22297.